Computer Methods in Biomechanics and Biomedical Engineering, 2002 Vol. 5 (3), pp. 195–206

A One-dimensional Finite Element Method for Simulation-based Medical Planning for Cardiovascular Disease

JING WAN[a], BROOKE STEELE[b], SEAN A. SPICER[b], SVEN STROHBAND[b], GONZALO R. FEIJÓO[b], THOMAS J.R. HUGHES[b] and CHARLES A. TAYLOR[b,c,*]

[a]*Department of Petroleum Engineering, Durand 213, Stanford University, Stanford, CA 94305-3030, USA;* [b]*Department of Mechanical Engineering, Durand 213, Stanford University, Stanford, CA 94305-3030, USA;* [c]*Department of Surgery, Durand 213, Stanford University, Stanford, CA 94305-3030, USA*

(Received 5 January 2001; In final form 14 June 2001)

We have previously described a new approach to planning treatments for cardiovascular disease, *Simulation-Based Medical Planning*, whereby a physician utilizes computational tools to construct and evaluate a combined anatomic/physiologic model to predict the outcome of alternative treatment plans for an individual patient. Current systems for Simulation-Based Medical Planning utilize finite element methods to solve the time-dependent, three-dimensional equations governing blood flow and provide detailed data on blood flow distribution, pressure gradients and locations of flow recirculation, low wall shear stress and high particle residence. However, these methods are computationally expensive and often require hours of time on parallel computers. This level of computation is necessary for obtaining detailed information about blood flow, but likely is unnecessary for obtaining information about mean flow rates and pressure losses. We describe, herein, a space–time finite element method for solving the one-dimensional equations of blood flow. This method is applied to compute flow rate and pressure in a single segment model, a bifurcation, an idealized model of the abdominal aorta, in three alternate treatment plans for a case of aorto-iliac occlusive disease and in a vascular bypass graft. All of these solutions were obtained in less than 5 min of computation time on a personal computer.

Keywords: Hemodynamics; Atherosclerosis; Computational methods; Surgical planning

INTRODUCTION

The determination of an appropriate therapy for an individual patient necessitates an assessment of alternate therapies on the basis of many factors including the patient's medical condition, expected tolerance to alternate procedures and the anticipated benefit of each treatment. In the case of occlusive cardiovascular disease, the determination of the benefit of a procedure is directly related to the expected improvement in blood flow. However, current methods for cardiovascular treatment planning, relying principally on diagnostic and empirical data, do not enable a physician to preoperatively assess the changes in blood flow for alternate therapies. Such predictions may be useful in evaluating and ranking different surgical procedures performed on patient specific models. We have previously described a simulation-based medical planning system for cardiovascular disease that uses computational methods to evaluate alternate options prior to treatment [1]. Three-dimensional analyses can provide detailed descriptions of local flow features (flow recirculation, shear stresses, particle residence time), but these analyses are both resource and time intensive. Consequently, three-dimensional pulsatile flow simulations are not suitable for the rapid evaluation of alternate surgical options.

Simpler, zero and one-dimensional methods have been used to describe blood flow in arteries and quantify mean flow rate and pressure. These models include lumped parameter models [2,3], one-dimensional linear pulse wave propagation methods solved using a frequency domain approach [4], and one-dimensional nonlinear pulse wave propagation methods solved using various numerical methods [5–9].

We have implemented a simulation-based medical planning system based on solving the one-dimensional nonlinear pulse wave propagation equations governing blood flow in the large systemic arteries using a finite element method. Although one-dimensional analyses do not provide the same level of flow detail that corresponding

*Corresponding author. Tel.: +1-650-725-6128. Fax: +1-650-498-6044. E-mail: taylorca@stanford.edu.

ISSN 1025-5842 print/ISSN 1476-8259 online © 2002 Taylor & Francis Ltd
DOI: 10.1080/10255840290010670

three-dimensional analyses do, they may yield adequate information to rank procedure outcomes. Our goal is to demonstrate that for similar geometry (one-dimensional and three-dimensional differences notwithstanding) we can rank outcomes of proposed surgical procedures in the same order as a fully three-dimensional simulation with our one-dimensional method in a small fraction of the time required for a three-dimensional calculation. This ranking will be based solely on flow rate and pressure, other factors such as shear stresses and recirculation will be ignored. We describe the space–time finite element formulation for solving the nonlinear evolution equations governing pulsatile blood flow in elastic vessels idealized as one-dimensional segments. Issues related to branching conditions and outflow boundary conditions are addressed and the implementation described. This method is applied to solve for pulsatile flow in a single segment, a symmetric bifurcation, an idealized abdominal aorta, three different surgical plans for a case of aorto-iliac disease and a porcine thoraco-thoraco aortic bypass. In the latter two examples, the computed flow rate is directly compared to the flow rate computed using three-dimensional methods. We demonstrate that a simplified one-dimensional blood flow problem can be solved roughly 5000 times faster than the three-dimensional one, thereby enabling the development and implementation of a rapid surgical design tool.

METHODS

Governing Equations (Strong Form)

The one-dimensional equations for the flow of a Newtonian fluid in a deforming, elastic domain consists of the continuity equation, a single axial momentum balance equation, a constitutive equation, and suitable initial and boundary conditions. The governing equations are derived in a general form by Hughes [6] and Hughes and Lubliner [10]. The partial differential equations for mass and momentum balance are given by

$$\frac{\partial S}{\partial t}+\frac{\partial Q}{\partial z}=-\psi \tag{1}$$

$$\frac{\partial Q}{\partial t}+\frac{\partial}{\partial z}\left((1+\delta)\frac{Q^2}{S}\right)+\frac{S}{\rho}\frac{\partial p}{\partial z}=Sf+N\frac{Q}{S}+\nu\frac{\partial^2 Q}{\partial z^2} \tag{2}$$

The primary variables are the cross-section area S and the volumetric flow rate Q. The density of the fluid is given by ρ (assumed constant), the external force by f, the kinematic viscosity by ν (assumed constant) and ψ is an outflow function (taken to be zero for impermeable vessels). The variables δ and N are defined by the choice of a profile function for the velocity over the cross-section. We define the fluid velocity by $V=\{V_1,V_2,V_3\}$, where V_3 is the component along the vessel axial direction, then construct a function ϕ, so that $V_3=\phi Q/S$. The variables δ and N are defined as

$$\delta=\frac{1}{S}\int_S(\phi^2-1)\mathrm{d}a \tag{3}$$

$$N=\oint_{\partial S}\frac{\partial\phi}{\partial m}\mathrm{d}l \tag{4}$$

where da is the cross-sectional area form, dl is the circumferential line element form, and m is the unit outward normal to the cross-sectional area. If we choose the profile to be axisymmetric and of the form

$$\phi(r)=\frac{n+2}{n}\left(1-\left(\frac{r}{R}\right)^n\right) \tag{5}$$

then we have

$$\delta=\frac{1}{1+n}\quad N=-2(n+2)\pi\nu \tag{6}$$

where r is the radial coordinate and R is the luminal radius. We assume a Poiseuille profile for our problem, and thus set $n=2$.

In regards to boundary conditions, we generally choose to specify the flow rate at the inlet(s) (Γ_{in})

$$Q(z,t)=Q^{\mathrm{in}}(t)\quad z\in\Gamma_{\mathrm{in}} \tag{7}$$

and either a prescribed pressure, flow rate, or a resistance boundary condition at the outlet(s) (Γ_{out})

$$p(z,t)=p^{\mathrm{out}}(t)\ \text{ or}$$

$$Q(z,t)=Q^{\mathrm{out}}(t)\ \text{ or}$$

$$p(z,t)-Q(z,t)R=0\quad z\in\Gamma_{\mathrm{out}} \tag{8}$$

where Q^{in}, p^{out} and Q^{out} are prescribed functions and R is the prescribed resistance at the outlet boundary.

The initial conditions for this problem are given by

$$S(z,0)=S^0(z),\quad Q(z,0)=Q^0(z) \tag{9}$$

where $S^0(z)$ and $Q^0(z)$ are prescribed functions.

Constitutive Equation

In order to complete the above system, we need to introduce a constitutive relationship. An elastic model is assumed which relates the pressure to the luminal area as follows:

$$p(z,t)=\hat{p}(S(z,t),z,t) \tag{10}$$

The particular constitutive relationship that we have used is that suggested by Olufsen [11]:

$$\hat{p}(S(z,t),z,t)=p^0(z)+\frac{4}{3}\frac{Eh}{r^0(z)}\left(1-\sqrt{\frac{S^0(z)}{S(z,t)}}\right) \tag{11}$$

where

$$p^0(z)=p(z,0) \tag{12}$$

$$r^0(z)=(S^0(z)/\pi)^{1/2} \tag{13}$$

and

$$\frac{Eh}{r^0(z)} = k_1 e^{k_2 r^0(z)} + k_3 \tag{14}$$

In this relationship, k_1, k_2, and k_3 are derived by a best fit to experimental data and are set to default values of $k_1 = 2 \times 10^7\ \mathrm{g \cdot s^{-2} \cdot cm^{-1}}$, $k_2 = -22.53\ \mathrm{cm^{-1}}$, and $k_3 = 8.65 \times 10^5\ \mathrm{g \cdot s^{-2} \cdot cm^{-1}}$.

Stenosis Model

In the presence of stenoses, the Poiseuille velocity profile assumption results in an underestimation of viscous losses [9]. In this case we have implemented an empirically based stenosis model. This is implemented by modifying the viscous loss term, N, given by $-8\pi\nu$ for the case of Poiseuille flow ($n = 2$). Seeley and Young [12] obtained an empirical formula for the pressure losses across models of arterial stenoses based on experimental data. It can be represented as follows:

$$\frac{\Delta p}{\rho V_0^2} = \frac{K_v}{Re_0} + \frac{K_t}{2}\left[\frac{S_0}{S_1} - 1\right]^2 \tag{15}$$

where

$$K_t = 1.52$$
$$K_v = 32\frac{L}{D_0}\left(\frac{S_0}{S_1}\right)^2 \tag{16}$$

and where here the subscript 0 refers to the vessel proximal to the stenosis, whereas the subscript 1 refers to the vessel in the stenosis. Re_0 is the Reynolds number, V_0 is the velocity, D_0 is the cross-sectional diameter, and L is the length of the stenosis.

This results in a modification to the viscous loss function N, of the form

$$N = \frac{-S_1^2 Q_0^2\left[\frac{K_v}{Re_0} + \frac{K_t}{2}\left(\frac{S_0}{S_1} - 1\right)^2\right]}{S_0^2 Q_1 L} \tag{17}$$

Quasi-linear Form

By noting that the pressure gradient can be expanded as

$$\frac{\partial p}{\partial z} = \frac{\partial \hat{p}}{\partial S}\frac{\partial S}{\partial z} + \frac{\partial \hat{p}}{\partial z} \tag{18}$$

we can rewrite the system of partial differential equations in a quasi-linear form:

$$\frac{\partial \mathbf{U}}{\partial t} + \mathbf{A}\frac{\partial \mathbf{U}}{\partial z} - \mathbf{K}\frac{\partial^2 \mathbf{U}}{\partial z^2} = \mathbf{G} \tag{19}$$

where

$$\mathbf{U} = \begin{bmatrix} U_1 \\ U_2 \end{bmatrix} = \begin{bmatrix} S \\ Q \end{bmatrix} \tag{20}$$

$$\mathbf{A} = \begin{bmatrix} 0 & 1 \\ -(1+\delta)\left(\frac{U_2}{U_1}\right)^2 + \frac{U_1}{\rho}\frac{\partial \hat{p}}{\partial S} & (1+\delta)\frac{2U_2}{U_1} \end{bmatrix} \tag{21}$$

$$\mathbf{K} = \begin{bmatrix} 0 & 0 \\ 0 & \nu \end{bmatrix} \tag{22}$$

$$\mathbf{G} = \begin{bmatrix} -\psi \\ Sf + N\frac{U_2}{U_1} - \frac{U_1}{\rho}\frac{\partial \hat{p}}{\partial z} \end{bmatrix} \tag{23}$$

Finite Element Method

We employ a stabilized space–time finite element method based on the discontinuous Galerkin method in time. The procedure presented herein employs ideas developed in Hughes and Mallet [13] and Hughes, Franca and Hulbert [14]. See also Brooks and Hughes [15] for background. So as not to distract from the applications focus of this paper, we present a brief overview of the method rather than a comprehensive theoretical exposition. The spatial discretization employs continuous piecewise linear polynomials whereas we use a piecewise constant temporal discretization. This method has been shown to yield stable, time-accurate solutions for advective–diffusive systems encountered in fluid mechanics.

The weak formulation of the initial boundary value problem is given as follows: Find $\mathbf{U}$ such that $\forall \mathbf{W} = [W_1 W_2]^T$,

$$\int_0^T\int_0^L (-\mathbf{W}_{,t}^T\mathbf{U} + \mathbf{W}^T\mathbf{A}\mathbf{U}_{,z} + \mathbf{W}_{,z}^T\mathbf{K}\mathbf{U}_{,z} - \mathbf{W}^T\mathbf{G})\mathrm{d}z\mathrm{d}t + \int_0^L \mathbf{W}^T(z,T)\mathbf{U}(z,T)\mathrm{d}z - \int_0^L \mathbf{W}^T(z,0)\mathbf{U}^0(z)\mathrm{d}z = 0 \tag{24}$$

where $\mathbf{U}^0(z) = [S^0(z), Q^0(z)]^T$. After discretizing in time, and assuming $\mathbf{U}$ and $\mathbf{W}$ are discontinuous across time slabs (i.e. $0 < z < L$, $t_n^+ \le t \le t_{n+1}^-$), we have

$$\int_{t_n^+}^{t_{n+1}^-}\int_0^L (-\mathbf{W}_{,t}^T\mathbf{U} + \mathbf{W}^T\mathbf{A}\mathbf{U}_{,z} + \mathbf{W}_{,z}^T\mathbf{K}\mathbf{U}_{,z} - \mathbf{W}^T\mathbf{G})\mathrm{d}z\mathrm{d}t + \int_0^L \mathbf{W}^T(z,t_{n+1}^-)\mathbf{U}(z,t_{n+1}^-)\mathrm{d}z - \int_0^L \mathbf{W}^T(z,t_n^+)\mathbf{U}(z,t_n^-)\mathrm{d}z = 0 \tag{25}$$

By using a piecewise constant approximation in time for both $\mathbf{U}$ and $\mathbf{W}$, the above equation can be simplified to

$$\Delta t_n\int_0^L (\mathbf{W}^T\mathbf{A}\mathbf{U}_{,z}^{n+1} + \mathbf{W}_{,z}^T\mathbf{K}\mathbf{U}_{,z}^{n+1} - \mathbf{W}^T\mathbf{G})\mathrm{d}z + \int_0^L \mathbf{W}^T(\mathbf{U}^{n+1} - \mathbf{U}^n)\mathrm{d}z = 0 \tag{26}$$

where the superscripts n and $n+1$ are identified with the solution at time instants t_n and t_{n+1}, and Δt_n is the time step. These equations are augmented by the addition of a stabilization term as follows.

We need to define a matrix $\mathbf{C} = \mathbf{C}(\mathbf{U})$ such that $\mathbf{CU} = \mathbf{G}$. To this end let

$$\mathbf{C}(\mathbf{U}) = \begin{bmatrix} -\frac{\psi}{U_1} & 0 \\ f - \frac{1}{\rho}\frac{\partial \hat{p}}{\partial z} & \frac{N}{U_1} \end{bmatrix} \tag{27}$$

With this we define a matrix differential operator by

$$\mathscr{L}(\mathbf{U}) = \mathbf{I}\frac{\partial}{\partial t} + \mathbf{A}(\mathbf{U})\frac{\partial}{\partial z} - \mathbf{K}\frac{\partial^2}{\partial z^2} - \mathbf{C}(\mathbf{U}) \tag{28}$$

Note that $\mathscr{L}(\mathbf{U})\mathbf{U}$ is the residual of the partial differential equation system, viz.

$$\mathscr{L}(\mathbf{U})\mathbf{U} = \mathbf{U}_{,t} + \mathbf{A}(\mathbf{U})\mathbf{U}_{,z} - \mathbf{K}\mathbf{U}_{,zz} - \mathbf{G}(\mathbf{U}) \tag{29}$$

For the case of a piecewise constant approximation in time and a piecewise linear approximation in space $\mathscr{L}(\mathbf{U})\mathbf{U}$ simplifies to

$$\mathscr{L}(\mathbf{U})\mathbf{U} = \mathbf{A}(\mathbf{U})\mathbf{U}_{,z} - \mathbf{G}(\mathbf{U}) \tag{30}$$

Note also that

$$\mathscr{L}(\mathbf{U})^T\mathbf{W} = \mathbf{A}(\mathbf{U})^T\mathbf{W}_{,z} - \mathbf{C}(\mathbf{U})^T\mathbf{W} \tag{31}$$

Therefore, the stabilization term takes the form:

$$\Delta t_n \sum_e \int_{\Omega_e} (\mathscr{L}(\mathbf{U})^T\mathbf{W})^T\boldsymbol{\tau}(\mathscr{L}(\mathbf{U})\mathbf{U})\mathrm{d}z \tag{32}$$

where the summation ranges over the element interiors and $\boldsymbol{\tau} = \boldsymbol{\tau}(\mathbf{U})$ is the stabilization matrix defined by:

$$\boldsymbol{\tau} = \left[\frac{2}{\Delta t_n}\mathbf{I} + \frac{2}{h}|\mathbf{A}| + 3\left(\frac{2}{h}\right)^2\mathbf{K} + |\mathbf{C}|\right]^{-1} \tag{33}$$

where the absolute value of a 2×2 matrix $\mathbf{B}$ can be obtained from the Cayley–Hamilton theorem, viz.

$$|B| = \frac{\mathbf{B}^2 + \sqrt{\det(\mathbf{B}^2)}\mathbf{I}}{\sqrt{\mathrm{tr}(\mathbf{B}^2) + 2\sqrt{\det(\mathbf{B}^2)}}} \tag{34}$$

Therefore the final variational form is given by: Find $\mathbf{U}^{n+1}$ such that $\forall \mathbf{W}$

$$\begin{aligned} &\Delta t_n \int_0^L (\mathbf{W}^T\mathbf{A}\mathbf{U}_{,z}^{n+1} + \mathbf{W}_{,z}^T\mathbf{K}\mathbf{U}_{,z}^{n+1} - \mathbf{W}^T\mathbf{G})\mathrm{d}z \\ &+ \int_0^L \mathbf{W}^T(\mathbf{U}^{n+1} - \mathbf{U}^n)\mathrm{d}z \\ &+ \Delta t_n \sum_e \int_{\Omega_e} (\mathbf{W}_{,z}^T\mathbf{A} - \mathbf{W}^T\mathbf{C})\boldsymbol{\tau}(\mathbf{A}\mathbf{U}_{,z}^{n+1} - \mathbf{G})\mathrm{d}z = 0 \end{aligned} \tag{35}$$

Assuming we have n nodal points in our spatial discretization, we can write the vector fields $\mathbf{W}$ and $\mathbf{U}^{n+1}$ as follows:

$$\mathbf{W} = \sum_{A=1}^{n} N_A\mathbf{C}_A$$

$$\mathbf{U}^{n+1} = \sum_{B=1}^{n} N_B\mathbf{U}_B^{n+1} \tag{36}$$

where $N_A(z)N_B(z)$ are the usual piecewise-linear shape functions. Using these definitions we can write a nonlinear vector valued function for all $\mathbf{C}_\mathrm{A}$'s:

$$\begin{aligned} \Re_A(\mathbf{U}^{n+1}) =& \Delta t_n \int_0^L \Bigg(N_A \sum_B N_{B,z}\mathbf{A}\mathbf{U}_B^{n+1} \\ &+ N_{A,z}\sum_B N_{B,z}\mathbf{K}\mathbf{U}_B^{n+1} - N_A\mathbf{G}\Bigg)\mathrm{d}z \\ &+ \int_0^L \left(N_A \sum_B N_B\left(\mathbf{U}_B^{n+1} - \mathbf{U}_B^n\right)\right)\mathrm{d}z \\ &+ \Delta t_n \sum_e \int_{\Omega_e} \left(N_{A,z}\mathbf{A} - N_A\mathbf{C}\right)\boldsymbol{\tau} \\ &\left(\sum_B N_{B,z}\mathbf{A}\mathbf{U}_B^{n+1} - \mathbf{G}\right)\mathrm{d}z = 0 \end{aligned} \tag{37}$$

where the subscript $A = 1, 2, \ldots, n$. This amounts to two algebraic equations at node A. For simplicity, we have suppressed the $\mathbf{U}^{n+1}$ argument in $\mathbf{A}$, $\mathbf{C}$, and $\mathbf{G}$.

We use a modified Newton–Raphson technique to solve this nonlinear system. The "modification" amounts to not using the consistent tangent by assuming that:

$$\frac{\partial \mathbf{A}}{\partial \mathbf{U}_C^{n+1}} = 0; \quad \frac{\partial \mathbf{C}}{\partial \mathbf{U}_C^{n+1}} = 0; \quad \frac{\partial \boldsymbol{\tau}}{\partial \mathbf{U}_C^{n+1}} = 0 \tag{38}$$

This means that we freeze the matrices $\mathbf{A}$, $\mathbf{C}$, and $\boldsymbol{\tau}$ in the calculation of the Jacobian. With this modification, the application of the Newton–Raphson method is facilitated by the following iterative scheme:

$$\begin{aligned} \sum_C \tilde{\mathbf{K}}_{AC}^{n+1,k}\delta\mathbf{U}_C^{n+1,k+1} &= -\Re_A^{n,k} \\ \mathbf{U}_C^{n+1,k+1} &= \mathbf{U}_C^{n+1,k} + \delta\mathbf{U}_C^{n+1,k+1} \end{aligned} \tag{39}$$

where the superscript k denotes the kth iteration and the

matrix $\tilde{\mathbf{K}}_{AC}$ is:

$$\begin{aligned}\tilde{\mathbf{K}}_{AC} &= \frac{\partial \Re_A}{\partial \mathbf{U}_C^{n+1}} \\ &= \Delta t_n \int_0^L (N_A \mathbf{A} N_{C,z} + N_{A,z} \mathbf{K} N_{C,z} - N_A \mathbf{C} N_C) \mathrm{d}z \\ &\quad + \int_0^L N_A \mathbf{I} N_C \mathrm{d}z + \Delta t_n \sum_e \int_{\Omega_e} (N_{A,z} \mathbf{A} \\ &\quad - N_A \mathbf{C}) \boldsymbol{\tau} (\mathbf{A} N_{C,z} - \mathbf{C} N_C) \mathrm{d}z \end{aligned} \tag{40}$$

Despite the modifications to the consistent tangent, we have observed rapid convergence of the iterative process.

Branch Points

At a connection of multiple segments, pressure continuity and conservation of mass are enforced using Lagrange multipliers. Without loss of generality, we assume for purposes of exposition there is one branch point. If we have m inlets and n outlets at the branch point l, then the following $m + n$ constraints must hold:

$$\begin{aligned} \sum_{C=1}^{m} Q_i^{\text{in}} - \sum_{C=1}^{n} Q_i^{\text{out}} &= 0 \\ p_C^{\text{in}} - p_l^{\text{in}} &= 0 \quad C = 2 \ldots m \\ p_C^{\text{out}} - p_l^{\text{in}} &= 0 \quad C = 1 \ldots n \end{aligned} \tag{41}$$

Recasting this information in terms of the Lagrange multipliers to form a potential function Z, we obtain:

$$\begin{aligned} Z &= \lambda_Q \left[\sum_{C=1}^{m} Q_C^{\text{in}} - \sum_{C=1}^{n} Q_C^{\text{out}} \right] \\ &\quad + \sum_{C=2}^{m} [\lambda_{p_{(C-1)}} (p_C^{\text{in}} - p_l^{\text{in}})] + \sum_{C=1}^{n} [\lambda_{p_{(C-1+m)}} (p_C^{\text{out}} - p_l^{\text{in}})] \end{aligned} \tag{42}$$

Besides the primary variable vector $\mathbf{U}$, $m + n$ Lagrange multipliers become additional unknowns of the nonlinear system. The corresponding new arrays in the global equation system can be expressed as follows:

$$\begin{aligned} \tilde{\mathbf{K}}_{Q_C,\lambda_Q} &= \tilde{\mathbf{K}}_{\lambda_Q,Q_C} = \frac{\partial^2 Z}{\partial Q_C \partial \lambda_Q}, \\ \tilde{\mathbf{K}}_{Q_C,\lambda_{p_D}} &= \tilde{\mathbf{K}}_{\lambda_{p_D},Q_C} = \frac{\partial^2 Z}{\partial Q_C \partial \lambda_{p_D}}, \\ \tilde{\mathbf{K}}_{S_C,\lambda_Q} &= \tilde{\mathbf{K}}_{\lambda_Q,S_C} = \frac{\partial^2 Z}{\partial S_C \partial \lambda_Q}, \\ \tilde{\mathbf{K}}_{S_C,\lambda_{p_D}} &= \tilde{\mathbf{K}}_{\lambda_{p_D},S_C} = \frac{\partial^2 Z}{\partial S_C \partial \lambda_{p_D}}, \\ \Re_{\lambda_Q} &= \frac{\partial Z}{\partial \lambda_Q}, \quad \Re_{\lambda_{p_D}} = \frac{\partial Z}{\partial \lambda_{p_D}} \end{aligned} \tag{43}$$

where $D = 1 \ldots n + m - 1$.

Contributions to existing arrays are denoted by $\leftarrow$ indicating that the expression on the right-hand side of the arrow should be added to the existing left-hand side.

$$\begin{aligned} \tilde{\mathbf{K}}_{S_C,S_D} &\leftarrow \frac{\partial^2 Z}{\partial S_C \partial S_D} \\ \Re_{Q_C} \leftarrow \frac{\partial Z}{\partial Q_C}, &\quad \Re_{S_C} \leftarrow \frac{\partial Z}{\partial S_C} \end{aligned} \tag{44}$$

Treatment of Boundary Conditions

After assembling the matrix $\tilde{\mathbf{K}}$, boundary conditions need to be enforced. The boundary conditions we have implemented are prescribed flow rate, prescribed pressure and a prescribed resistance (linear relationship between pressure and flow rate). To enforce the flow rate boundary condition, the equation for that degree-of-freedom is replaced by an equation representing the boundary condition, and the Newton–Raphson method is applied in the same way as discussed previously. If we denote the node for which the prescribed flow rate boundary condition is to be applied by an index C, the residual is defined by

$$\Re_{Q_C} = Q_C^{n+1} - Q_C^{\text{in}}(t_{n+1}) = 0 \tag{45}$$

where $Q_C^{\text{in}}(t_{n+1})$ is the prescribed flow rate. The row and column in the matrix $\tilde{\mathbf{K}}$ corresponding to variable Q_C are set to zero, and the diagonal component corresponding to that degree-of-freedom is set to 1, i.e.

$$\tilde{\mathbf{K}}_{Q_C,Q_C} = 1 \tag{46}$$

The pressure boundary condition must first be translated into a luminal area boundary condition. The area residual is then

$$\Re_{S_C} = S_C^{n+1} - \hat{S}(p_C^{\text{out}}(t_{n+1}), z_C, t_{n+1}) = 0 \tag{47}$$

where $\hat{S}$ is obtained by inverting the pressure constitutive relation (11). We then proceed as in the case of the flow rate boundary condition, namely, we set

$$\mathbf{K}_{S_C,S_C} = 1 \tag{48}$$

and zero the terms in the row and column of $\tilde{\mathbf{K}}$ corresponding to degree-of-freedom S_C.

The resistance boundary condition amounts to a constraint between flow rate and pressure (hence luminal area). This can be written in terms of the flow rate residual:

$$\Re_{Q_C} = Q_C^{n+1} - \hat{p}(S_C^{n+1}, z_C, t_{n+1}) R^{-1} \tag{49}$$

Linearization about the kth iterative state yields

$$\delta Q_C^{n+1,k+1} = \frac{\partial \hat{p}}{\partial S}(S_C^{n+1,k}, z_C, t_{n+1}) \delta S_C^{n+1,k+1} R^{-1} \tag{50}$$

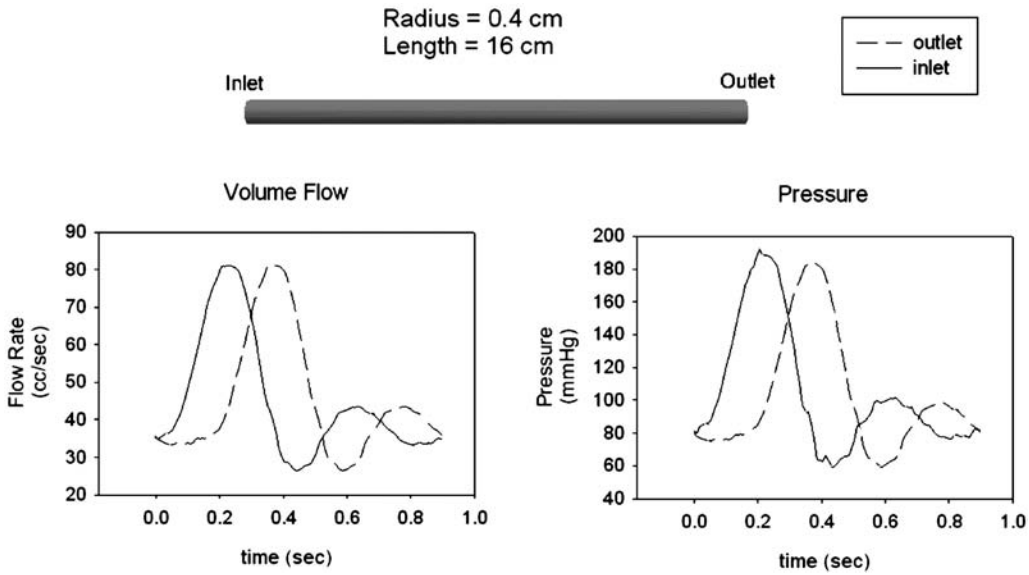

FIGURE 1 Problem description and results for single segment model with uniform cross-section and material properties. Volume flow rate is specified at the inlet and a resistance boundary condition was specified at the outlet of the single segment model. Note the propagation of the flow and pressure waves with little damping or dispersion.

For future reference, we write

$$\alpha = \frac{\partial \hat{p}}{\partial S}(S_C^{n+1,k}, z_C, t_{n+1})R^{-1} \tag{51}$$

These relations imply the following alterations to the matrix system: The residual of the Q_C degree-of-freedom, $\Re_{Q_C}$ is given above. The residual of the S_C equation, $\Re_{S_C}$, needs to be modified by the addition of $\alpha\Re_{Q_C}$. The Q_C row of the matrix $\tilde{\mathbf{K}}$ needs to be multiplied by α and added to the S_C row. Subsequently, the Q_C column needs to be multiplied by α and added to the S_C column. Then we define

$$\tilde{\mathbf{K}}_{Q_C,Q_C} = 1 \tag{52}$$

and zero the remaining terms of the Q_C row and column to complete the specification of the resistance boundary condition.

RESULTS

We first consider pulsatile flow in an elastic tube with a prescribed flow rate at the inlet and resistance boundary conditions at the exit. The dimensions of this vessel were chosen to correspond approximately to that of the human common carotid artery. Specifically, the nominal radius was specified to be 0.4 cm and the vessel length was specified to be 16 cm (length to diameter ratio of 20). A total of 16 finite elements were utilized and the solution was computed using 100 time steps per cardiac cycle for a total of three cardiac cycles. Figure 1 depicts the results obtained. We note that the volume flow rate and pressure waves are propagated down the length of the vessel with little damping or dispersion.

We next consider pulsatile flow in a symmetric bifurcation with equal resistances at the two outlets. The dimensions of this vessel were chosen to correspond approximately to the human aortic bifurcation. The model consisted of 50 elements with the element size of 1 cm; 16 elements in the inlet branch and 17 each in the left and right branches. The solution was computed using 100 time steps per cardiac cycle for a total of three cardiac cycles. Figure 2 depicts the results obtained. The volume flow rates and pressure waves are identical for the right and left branches. Furthermore, although not shown, the pressure at the exit to the inlet branch is identical to the pressure at the inlet of each of the branches and the volume flow rate is conserved across the junction.

We next consider pulsatile flow in an idealized abdominal aorta with varying vessel dimensions and outlet resistances, but uniform material properties. The volume flow rate is specified at the inlet boundary and resistances are specified at all the exits. The exit resistances were chosen so that the mean flow rate in each of the branches corresponds to the three-dimensional pulsatile flow calculations described by Taylor *et al.* [16]. Figure 3 depicts the volume flow rate and pressure at the inlet and all of the outlets of the idealized abdominal aorta model. The blood flow distribution is nonuniform due to the differing terminal resistances and cross-sectional areas. We also note that the pressure and flow are in phase at the exit in accordance with a purely resistive boundary condition.

We finally consider pulsatile flow in a model of a treatment for aorto-iliac occlusive disease. For this problem, the right iliac artery is completely occluded, the left iliac artery has a 50% reduction in diameter, the

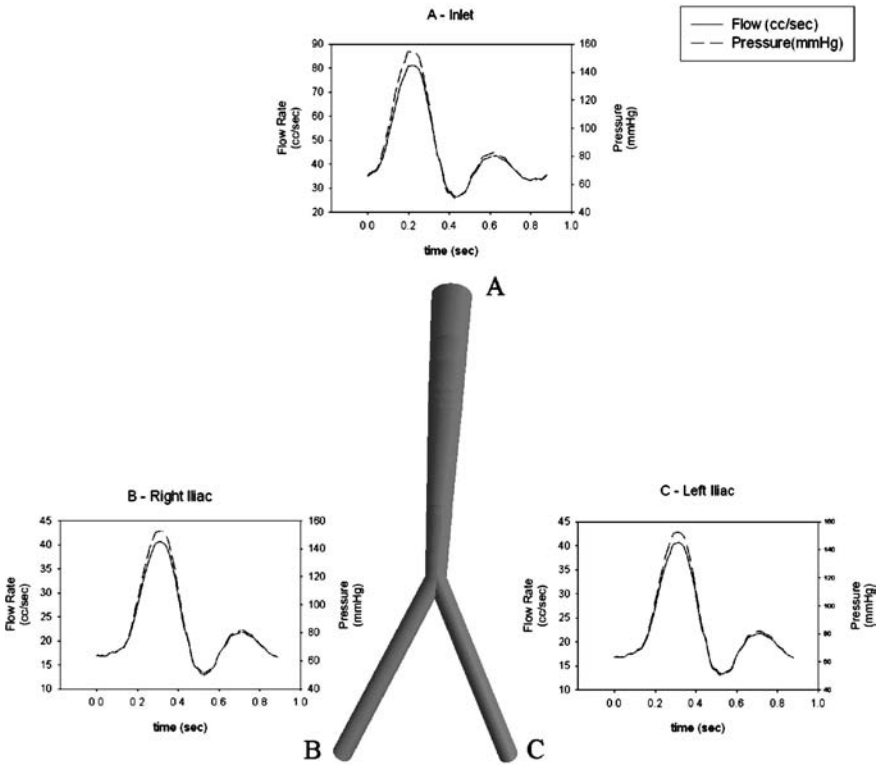

FIGURE 2 Problem description and results for symmetric bifurcation segment model. Volume flow rate is conserved at the branch point and pressure is continuous. Note that the exit pressures and flow rates are identical for the two branch vessels.

right superficial femoral artery has a series of stenoses and the left superficial femoral artery is completely occluded. We previously solved this problem using a three-dimensional finite element method in a preoperative model and three alternate treatment plans: an aorto-femoral bypass procedure with a proximal end-to-side anastomosis, an aorto-femoral bypass procedure with a proximal end-to-end anastomosis (shown in Fig. 4), and angioplasty with a femoral-to-femoral bypass graft [1].

TABLE I Comparison between volumetric flow rate at various locations for one-dimensional and three-dimensional methods for preoperative case and three alternate treatment plans

Flow (cc/s)	1D	3D	Difference (%)
Preoperative			
Aorta	50.10	50.15	0
R femoral	2.29	3.60	−36
L femoral	7.76	7.73	0
R popliteal	1.21	0.50	142
L popliteal	4.58	4.53	1
Angioplasty with Fem–Fem bypass			
Aorta	57.64	57.67	0
R femoral	6.67	7.40	−10
L femoral	15.72	12.45	26
R popliteal	3.75	2.70	39
L popliteal	5.34	4.83	10
AFB with end to end anastomosis			
Aorta	57.64	57.67	0
R femoral	8.98	10.25	−12
L femoral	6.79	9.17	−26
R popliteal	5.05	4.72	7
L popliteal	5.72	5.85	−2
AFB with end to side anastomosis			
Aorta	57.64	57.67	0
R femoral	8.24	11.05	−25
L femoral	8.07	13.02	−38
R popliteal	4.64	5.15	−10
L popliteal	5.66	6.03	−6

Resting flow conditions were used to assess the blood flow in the foot needed for wound healing. The boundary conditions for preoperative and postoperative computations were prescribed as follows. First, preoperative analyses under resting flow conditions were performed with a specified volume flow rate through each boundary based on literature data for flow distribution [16]. This preoperative analysis was used to compute the average pressure distribution at each outflow boundary. Second, the resistance was computed for each outflow boundary based on a relationship between pressure and volume flow rate of the form $p = QR$, where p is the mean pressure, Q is the volume flow rate and R is the resistance to flow. Using this strategy, the volume flow rate Q and pressure p were calculated (not specified) for each of the boundaries for each of the surgical plans. Stenoses were accounted for by the model described previously. The nonlinear evolution equations governing blood flow for each treatment plan were then solved for the velocity and pressure fields over five cardiac cycles with 200 time steps per cardiac cycle. Figure 4 depicts the results for one of the surgical plans, the aorto-femoral bypass with a proximal end-to-end anastomosis. Table I depicts the mean flow rate for the preoperative case and all three alternate

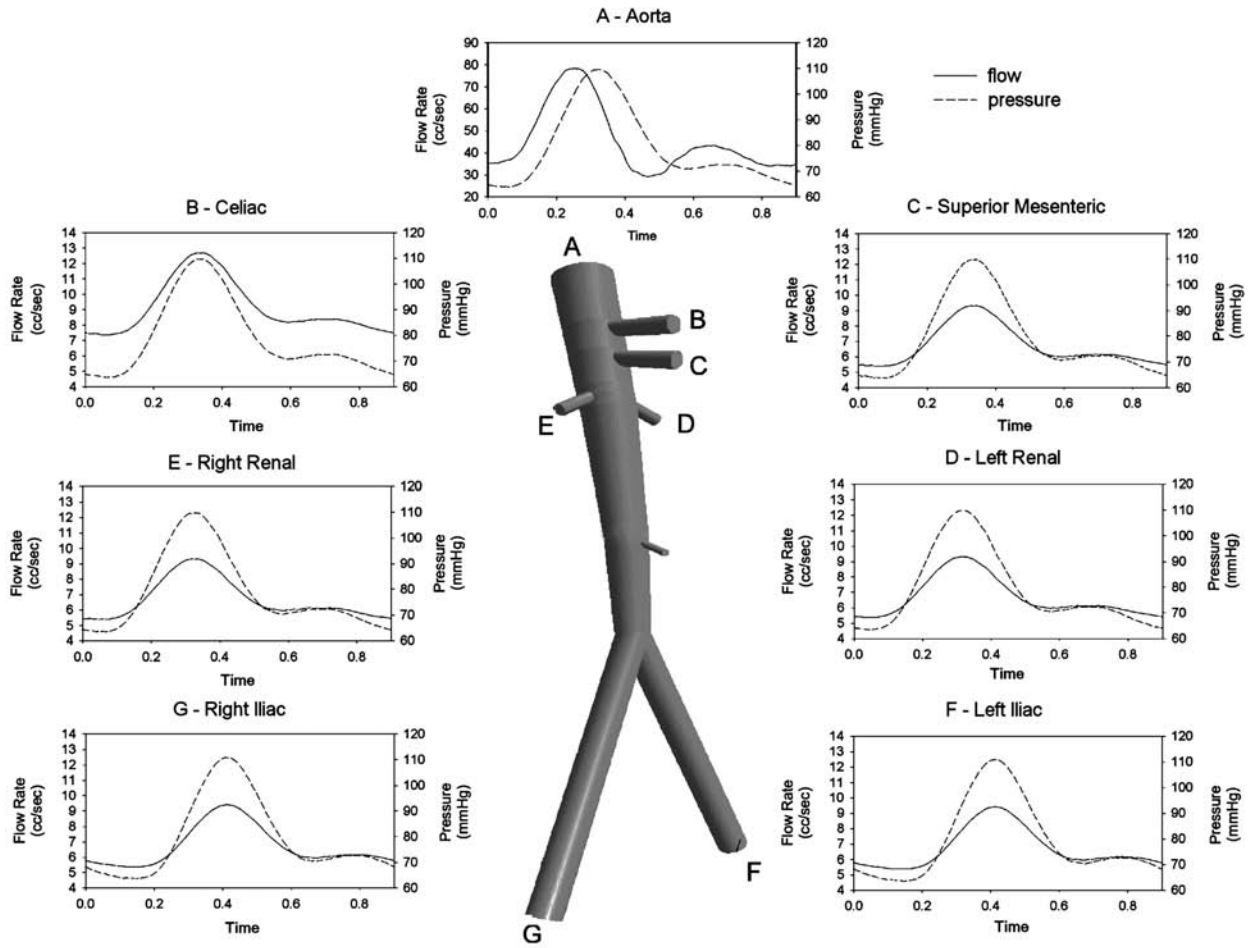

FIGURE 3 Problem description and results for idealized abdominal aorta with varying vessel dimensions and outlet resistances, but uniform material properties. Volume flow rate and pressure are depicted at inlet and outlets of idealized abdominal aorta model.

surgical procedures computed using the one-dimensional method described in this paper and our previously published three-dimensional method [1]. Overall, the one-dimensional solutions compare favorably to the three-dimensional solutions. The three-dimensional solutions involved approximately 500,000 degrees-of-freedom and approximately 25,000 cpu minutes of solution time whereas the one-dimensional solutions required less than 500 degrees-of-freedom and less than 5 cpu minutes of solution time. With respect to the cost of model preparation, the three-dimensional model is based on an analytic solid model and three-dimensional finite element mesh and requires days of preparation time whereas the one-dimensional model and mesh can generally be created in less than 1 h.

The final problem we consider is the pulsatile flow through a porcine thoraco-thoraco aortic bypass graft as shown in Fig. 5. The pressure and flow rate at the inlet, native aorta, bypass graft and outlet are displayed. The peak differences between the three-dimensional and one-dimensional methods are on the order of 50% in the native aorta, but less than 10% in the bypass graft. The stenosis model described previously was not used in this simulation.

DISCUSSION

We have described a space–time finite element formulation for solving the nonlinear evolution equations governing pulsatile blood flow in elastic vessels. This method, based on well-established methods for advective–diffusive systems common in fluid mechanics, includes the enforcement of pressure continuity and mass conservation at branch points as well as flow rate, pressure and resistance boundary conditions. The resulting system of nonlinear equations is solved using a Newton–Raphson method. The solution of the one-dimensional blood flow equations in a single segment reveals the propagation of the flow waveform with negligible change and the propagation of the pressure wave with little damping and dispersion. The application of this method to flow in a symmetric bifurcation demonstrates the accurate enforcement of the branch conditions as well as the expected symmetric solution. Pulsatile flow in an idealized model of the human aorta demonstrates the application to models with multiple branches. The primary motivation behind this research is simulation-based medical planning, and this method is applied to simulate blood flow in three different surgical plans for a case of

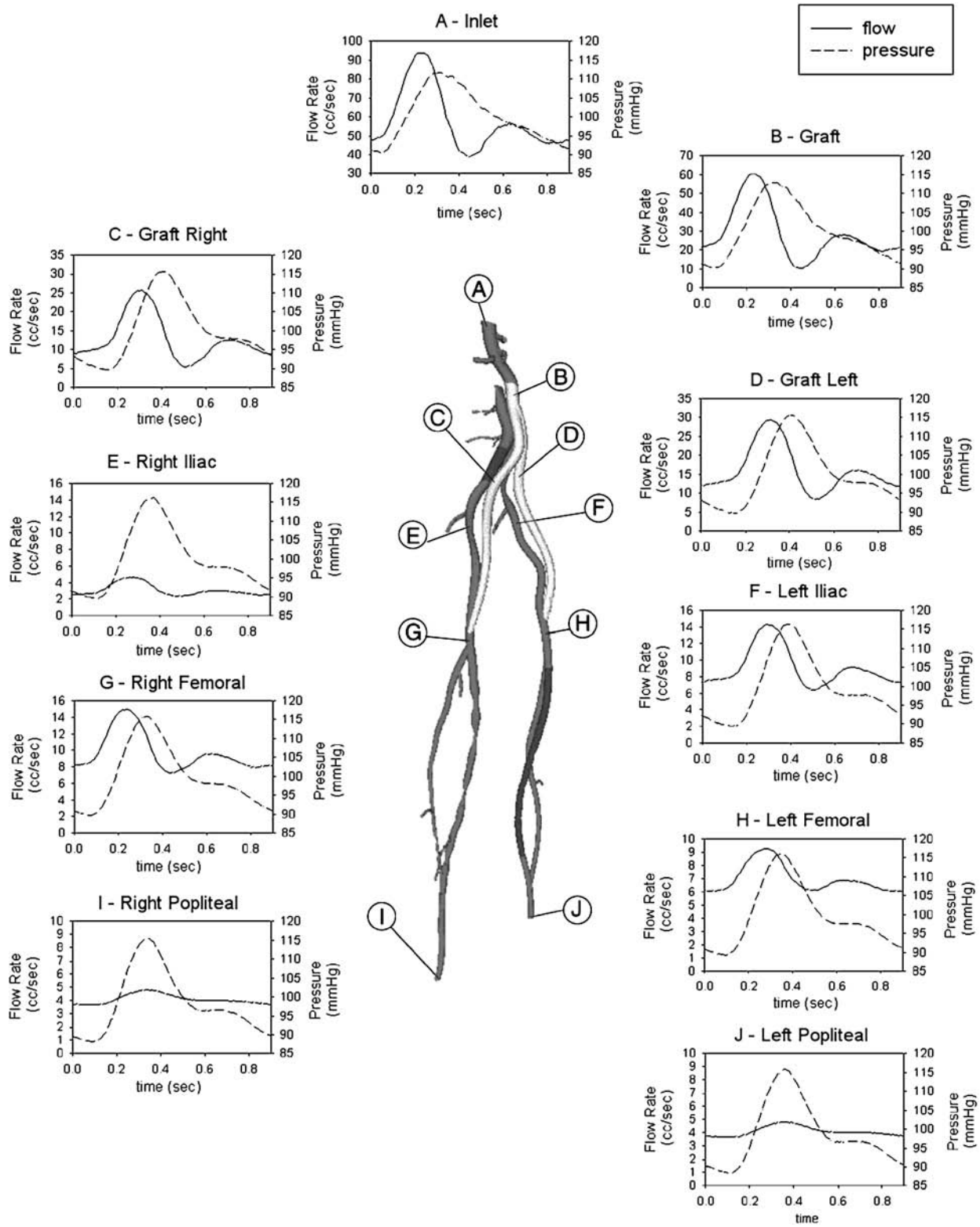

FIGURE 4 Problem description for case of aorto-iliac occlusive disease treated with aorto-femoral bypass graft with proximal end-to-end anastomosis. Volume flow rate and pressure are depicted at inlet, outlets and representative locations of treatment plan.

aorto-iliac disease and blood flow in a porcine thoraco-thoraco aortic bypass. For the simulation of blood flow in the treatment plans for a case of aorto-iliac occlusive disease, we observed overall good agreement between the one-dimensional solution and previously computed three-dimensional solutions using the same output resistance boundary conditions. In the case of blood flow in a porcine thoraco-thoraco aortic bypass, we also obtained good agreement between the one-dimensional solutions and three-dimensional solutions. Either the neglect of three-

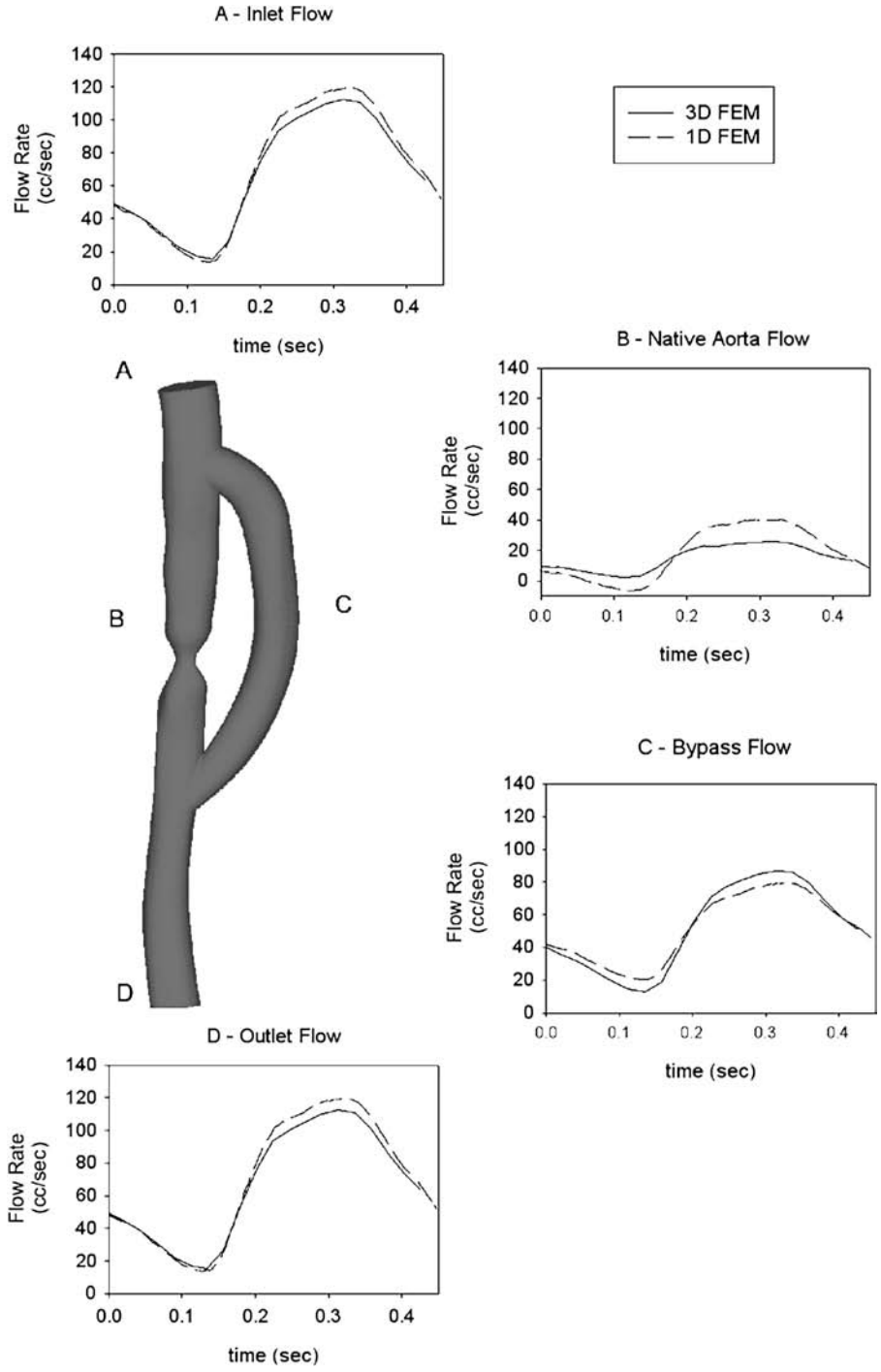

FIGURE 5 Problem description for case of pulsatile flow in vascular bypass graft. Volume flow rate for three-dimensional and one-dimensional methods are depicted at the inlet, in the aorta above the stenosis, in the bypass graft and the outlet.

dimensional effects for the one-dimensional method or the neglect of wall compliance for the three-dimensional models could explain the observed differences. Further analysis and comparisons with experiment are needed to resolve this question.

The major assumptions employed in this investigation include the assumption of elastic walls, Newtonian viscosity, exit boundary conditions, and the one-dimensional approximation to blood flow and the resulting choice of the cross-sectional velocity profile function. The utilization of these assumptions is believed to constitute a reasonable approximation to the actual mechanics of blood flow in large arteries and must be evaluated in the context of the goal of developing a rapid design tool for cardiovascular treatment planning.

The elastic approximation to the true viscoelastic character of blood vessels is expected to be sufficient to represent the pulse propagation in the one-dimensional domain to a first approximation. A Newtonian constitutive model for viscosity was employed in the present

investigation and is generally accepted as a reasonable first approximation to the actual behavior of blood at shear rates observed in large arteries [17]. However, future studies could include non-Newtonian rheologic models.

The one-dimensional approximation to blood flow ignores secondary flows present due to curvature, taper, expansions, and branching. These more complex flow fields induce viscous losses that are not well approximated by the assumed Poiseuille velocity profile. However, as in the case of the stenosis model, the viscous loss function can be modified using empirical models in regions where secondary flows are anticipated. Further validation of the one-dimensional approximation to blood flow using three-dimensional methods and experimental data could help in the development of these empirical models.

In regards to the solution of pulsatile blood flow, the outflow boundary conditions represent the most significant determinant of the resulting flow rate and pressure propagation for problems with multiple outlets. We described the implementation of flow rate, pressure and resistance boundary conditions, but the resistance boundary condition is utilized in most cases. Pressure and flow rate waveforms are, in general, not known *a priori* and the resistance of a vascular bed can be used to represent downstream conditions. This approach is limited in that a purely resistive model does not reflect the actual relationship between pressure and flow rate due to the pulsatile nature of blood flow in compliant vessels. In particular, pure resistive boundary conditions force the pressure and flow rate to be in phase, a condition that rarely applies in the vascular system. More appropriate boundary conditions can be derived using lumped parameter or Windkessel models. For example, Stergiopulos *et al.* [9] use a modified Windkessel model to account for the capacitive and resistive effects of the vasculature at the exits of a one-dimensional wave propagation model. These boundary conditions result in an ordinary differential equation relating pressure and flow. The difficulty with these methods lies in the fact that these lumped methods cannot account for the true wave-like characteristics of blood flow in the vascular bed and further that there is no direct physical relationship between changes in the anatomic dimensions of the distal bed and the parameters of the model.

An improved approach to boundary conditions can be derived using the concept of vascular impedance. The impedance, defined as the ratio of the harmonic terms of pressure and flow, is a measure of the opposition to flow, and can be calculated from measured pressure and flow waveforms. The impedance reflects the downstream conditions of a vascular bed and when applicable is an excellent boundary condition to apply at the outflow branches of arterial models. Olufsen [11] described a combined one-dimensional wave transmission and impedance approach whereby a finite difference method is used to solve the nonlinear wave transmission equations in a model of the major arteries and a fractal branched network is used to represent the distal vascular beds for each of the outlets of the wave transmission model. The input impedance of the vascular beds is calculated in the frequency domain, the inverse Fourier transform of the impedance is calculated, and then a convolution integral is used to determine the relation between pressure and flow rate. We are currently implementing impedance boundary conditions into our methods for solving the one-dimensional equations of blood flow. It is anticipated that this approach will yield outflow boundary conditions that more accurately reflect actual conditions.

In spite of the assumptions that underlie the one-dimensional model of blood flow, it is likely that simulation-based medical planning systems based upon the solution of these equations will be valuable for rapid evaluation of alternate treatment plans. Ultimately, systems that combine one-dimensional and three-dimensional methods will enable physicians to design therapeutic procedures that yield improved blood flow to patients with cardiovascular disease.

Acknowledgements

The authors gratefully acknowledge the support and assistance of Joy Ku in obtaining the three-dimensional solutions for the vascular bypass graft. Charles A. Taylor and Brooke Steele were supported by the Whitaker Foundation.

References

[1] Taylor, C.A., Draney, M.T., Ku, J.P., Parker, D., Steele, B.N., Wang, K.C. and Zarins, C.K. (1999) "Predictive medicine: computational techniques in therapeutic decision-making", *Computer Aided Surgery* **4**, 231–247.

[2] Pater, L. and van den Berg, J.W. (1964) "An electrical analogue of the entire human circulatory system", *Medical Electronics and Biological Engineering* **2**, 161–166.

[3] Westerhof, N., Bosman, F., De Vries, C.J. and Noordergraaf, A. (1969) "Analog studies of the human systemic arterial tree", *Journal of Biomechanics* **2**, 121–143.

[4] Avolio, A.P. (1980) "Multi-branched model of the human vascular system", *Medical and Biological Engineering and Computing* **18**, 709–718.

[5] Anliker, M., Rockwell, L. and Ogden, E. (1971) "Nonlinear analysis of flow pulses and shock waves in arteries", *ZAMP* **22**, 217–246.

[6] Hughes, T.J.R. (1974). "A Study of the One-Dimensional Theory of Arterial Pulse Propagation," Report No. 74-13, Division of Structural Engineering and Structural Mechanics, Department of Civil Engineering, U.C. Berkeley, (available from the author).

[7] Hillen, B., Hoogstraten, H.W. and Post, L. (1986) "A mathematical model of the flow in the circle of Willis", *Journal of Biomechanics* **19**, 187–194.

[8] Reuderink, P.J., Hoogstraten, H.W., Sipkema, P., Hillen, B. and Westerhof, N. (1989) "Linear and nonlinear one-dimensional models of pulse wave transmission at high Womersley numbers", *Journal of Biomechanics* **22**, 819–827.

[9] Stergiopulos, N., Young, D.F. and Rogge, T.R. (1992) "Computer simulation of arterial flow with applications to arterial and aortic stenosis", *Journal of Biomechanics* **25**, 1477–1488.

[10] Hughes, T.J.R. and Lubliner, J. (1973) "On the one-dimensional theory of blood flow in the larger vessels", *Mathematical Biosciences* **18**, 161–170.

[11] Olufsen, M. (1999) "Structured tree outflow condition for blood flow in larger systemic arteries", *American Journal of Physiology* **276**, 257–268.

[12] Seeley, B.D. and Young, D.F. (1976) "Effects of geometry on pressure losses across models of arterial stenoses", *Journal of Biomechanics* **9**, 439–448.

[13] Hughes, T.J.R. and Mallet, M. (1986) "A new finite element method for computational fluid dynamics: III. The generalized streamline operator for advective–diffusive systems", *Computer Methods in Applied Mechanics and Engineering* **58**, 305–328.

[14] Hughes, T.J.R., Franca, L.P. and Hulbert, G.M. (1989) "A new finite element method for computational fluid dynamics: VIII The Galerkin/least squares method for advective–diffusive equations", *Computer Methods in Applied Mechanics and Engineering* **73**, 173–189.

[15] Brooks, A.N. and Hughes, T.J.R. (1982) "Streamline upwind Petrov-Galerkin formulation for convection dominated flows with particular emphasis on the incompressible Navier Stokes equations", *Computer Methods in Applied Mechanics and Engineering* **32**, 199–259.

[16] Taylor, C.A., Hughes, T.J.R. and Zarins, C.K. (1998) "Finite element modeling of 3-dimensional pulsatile flow in the abdominal aorta: relevance to atherosclerosis", *Annals of Biomedical Engineering* **26**, 1–14.

[17] Perktold, K., Peter, R.O., Resch, M. and Langs, G. (1991) "Pulsatile non-Newtonian flow in three-dimensional carotid bifurcation models: a numerical study of flow phenomena under different bifurcation angles", *Journal of Biomedical Engineering* **13**, 507–515.